Results in Physics 6 (2016) 712–718

Contents lists available at ScienceDirect

Results in Physics

journal homepage: www.journals.elsevier.com/results-in-physics

Neem leaves mediated preparation of NiO nanoparticles and its magnetization, coercivity and antibacterial analysis

V. Helan [a], J. Joseph Prince [a,*], Naif Abdullah Al-Dhabi [b], Mariadhas Valan Arasu [b], A. Ayeshamariam [c,*], G. Madhumitha [d], Selvaraj Mohana Roopan [d,*], M. Jayachandran [e]

[a] Research and Development Centre, BIT Campus, Anna University of Technology, Tiruchirappalli 623024, India
[b] Department of Botany and Microbiology, Addiriyah Chair for Environmental Studies, College of Science, King Saud University, P.O. Box 2455, Riyadh 11451, Saudi Arabia
[c] Department of Physics, Khadir Mohideen College, Adirampattinam 614701, India
[d] Chemistry of Heterocycles and Natural Product Research Laboratory, Department of Chemistry, School of Advanced Sciences, VIT University, Vellore 632014, Tamil Nadu, India
[e] Department of Physics, Sree Sevugan Annamalai College, Devakottai, 630303, India

ARTICLE INFO

Article history:
Received 23 September 2016
Received in revised form 6 October 2016
Accepted 10 October 2016
Available online 14 October 2016

Keywords:
Neem seed
NiO NPs
Coercivity
Magnetic properties
Bacterial activities

ABSTRACT

Nickel oxides nanoparticles (NiO NPs) were synthesized by biosynthesis method with the help of phyto-constituents present in the neem leaf. Further the synthesized NiO NPs were subjected for structural, optical, morphological and magnetic properties. The XRD patterns clearly infer the presence of polycrystalline nature of samples (0 1 0), (0 1 1) and (0 1 2) with hexagonal crystal phase. Morphological studies using Transmission Electron Microscope (TEM) reveals that the biosynthesized NiO NPs were in shape of oblong with 12 nm in size. Elemental analysis (EDAX) confirms the quantity of Ni is present at 51% and remaining O as 49% as well as the mass magnetization values of 61 emu/g are also recorded for NiO NPs and its coercivity values in the range of 0.2–0.4 of nanoparticles respectively. Finally the NiO NPs was studied for bacterial activity against *Staphylococcus aureus* (MTCC 1430) and followed by *Escherichia coli* (MTCC 739) by agar diffusion assay.

Introduction

For the past few years, nanoscience and nanotechnology have developed tremendously due to its wide application. The eco-friendly synthesis has also grown since there are wide scopes. The synthesize was categorized into top to bottom and bottom-up approaches [1]. Semiconducting oxide nanomaterials possess antibacterial, antifungal and biological activities [2]. Various researchers have prepared the nontoxic material by different plant extractions like *Annona squamosa* [3–6], *Catharanthus roseus* [7], *Cocos nucifera* [1,8], *Beta vulgaris* [9], *Catunaregam spinosa* [10], *Cyphomandra betacea* [11], etc., usually plant extracts contains variety of compounds with different functional groups [11–15] which are for many chemicals and biological applications. During the nanoparticles metabolites play a crucial role in converting metal into metal nano form by reduction mechanism [16]. Specialization of NPs are its porosity, high surface area, very small crystal size random distribution of semiconducting oxide materials, particularly this stable group of oxide materials are having the huge coercivity applications while matched with powder layered particles [17]. The coercivity magnitude of nanoparticles decreases with the increase in the size of the particles with relation to magnetic hysteresis curve. In this manuscript we have stated the biosynthesis of NiO NPs with different annealing temperatures and its magnetic properties. The NiO NPs prepared were of cubic face centered, the crystalline size of nanoparticles increases with increase in temperature [18]. The NiO NPs have unique property of converting the anti-paramagnetic to ferromagnetic one in room temperature itself [19]. So in this manuscript we focused our research toward green synthesis of NiO NPs using neem leaves and it was augmented against various toxic pathogens.

Experimental

Materials

Nickel chloride salt ($NiCl_2$) were the starting material for synthesis of NiO NPs were bought from Merck chemical industries, Mumbai, India. The NaOH were acquired from AVRA Synthesis, Hyderabad, India. The fresh Neem leaves were collected from in and around Anna University, BIT campus, Tiruchirappalli. Bacterial

* Corresponding authors.
E-mail addresses: selvarajmohanaroopan@gmail.com, mohanaroopan.s@vit.ac.in (S.M. Roopan).

http://dx.doi.org/10.1016/j.rinp.2016.10.005
2211-3797/

culture was obtained from MTCC, India. Further throughout the experiments we have utilized milli Q water and double distilled water without any further purification.

Collection of neem leaf extract

Freshly collected neem leaves were crushed using mortar pestle until it turns into greeny paste solution. Further crushed solutions were transferred for centrifugation process to remove debris at 10,000 rpm for 10 min with controlled temperature of 4–5 °C. After centrifugation the supernatant was taken and by using filter paper (Whatmann No. 1), further the collected residue were utilized as phyto precursors for production of NiO NPs.

Preparation of NiO NPs by method of bio-synthesis

The NaOH (1 mM, Reagent A) were prepared individually and mixed with 1 μL of neem leaf extract which was prepared in 30 μL of milli Q water (Reagent B). Both the reagents were mixed thoroughly by heating it in 200 °C for 20 min. Further it was then filtered and the residue was collected separately (Reagent C) [20].

This reagent C was mixed well the aqueous solution of Nickel chloride with varying the pH. The volumetric ratio mixture of extract and Nickel chloride salt was 4/100. In this reaction the control experiment consists of Nickel chloride solution.

The NiO NPs were prepared by using the neem leaf extract. Then the extract was mixed with the nickel chloride. We have observed immediate color change in the solution which may be due to the formation of NiO NPs.

Before the synthetic process, various optimizations of the conditions were checked and it was concluded that the volume of neem extract used as 1 μL, pH maintained at 7 and the time taken for the reaction is 20 min at constant stirring. By using the above parameters, we have synthesized the nanoparticles and the solutions were checked in spectrophotometer for the nanoparticle form [21].

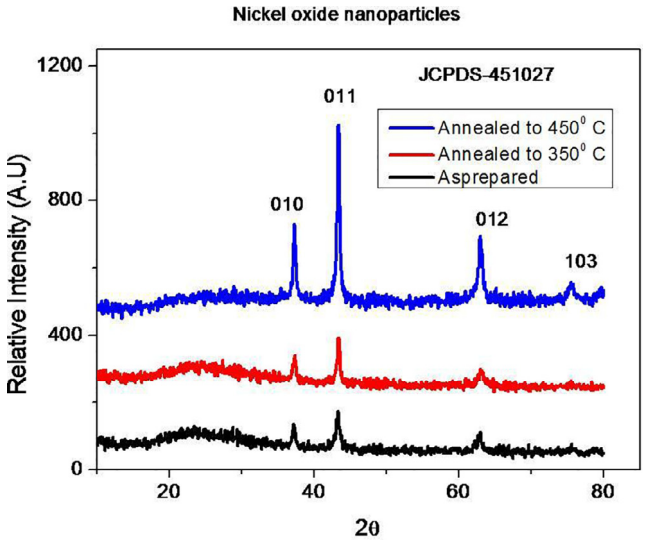

Fig. 1. XRD analysis of NiO and its two different annealing temperatures.

NiO NPs characterization and applications

Further bio-synthesized NiO NPs were subjected for its structural, optical, morphological studies with the help of various analytical techniques like XRD, FTIR, SEM/EDAX and TEM. Once the analytical process has done, further bio-synthesized NiO NPs were subjected for magnetic and bacterial properties which were briefly discussed in results and discussion part.

Results and discussion

XRD of biosynthesized NiO NPs

The XRD pattern of NiO NPs were annealed under (350 and 450 °C) which are shown in Fig. 1. Resulted diffraction peaks are indexed within Face Centered Cubic (FCC) structure of NiO phase with respective agreement with JCPDS card No. 451027 (Hexagonal). Broad peaks indicate the formation of NiO nanocrystalline phase. The crystalline size (D), density of dislocation (δ), strain (ε), lattice parameter (a), are calculated by formulae denoted here.

$$D = \frac{0.9\lambda}{\beta cos\theta} \tag{1}$$

where wavelength is λ, β is FWHM in radian and angle of Braggs denoted by θ, the dislocation parameter is derived using following formulae;

$$\delta = \frac{1}{D^2} \tag{2}$$

The strain is then determined by the following relation,

$$\varepsilon = \frac{\Delta d}{d_o} = \left(\frac{d_{exp} - d_{hkl}}{d_{hkl}}\right) \tag{3}$$

Table 1
Structural analysis of NiO Nanoparticles annealed at 350 °C and at 450 °C.

Sample	Lattice constant calculated (Å)	Crystal size size D = $\frac{0.94\lambda}{\beta Cos\theta}$ (nm)	Strain $\frac{\Delta d}{d_o} = \left(\frac{d_{exp} - d_{hkl}}{d_{hkl}}\right) \times 10^{-3}$ lines/m^2	Band gap (eV)
NiO	a = 2.701 c = 4.412	29.823	1.269	3.22
350 °C	a = 2.698 c = 4.439	32.14	1.331	3.12
450 °C	a = 2.711 c = 4.440	33.24	1.401	3.01

Table 2
EDAX analysis of NiO nanoparticles as prepared sample.

Element	Net counts	ZAF	Weight %	Atom	Formula
Ni	0	8.633	0.00	0.00	Ni
O	3220	7.599	34.25	68.64	O
Ni	1116	2.699	1.32	1.74	Ni
O	17,263	1.604	13.49	15.40	O
Ni	37,509	1.185	50.94	14.23	Ni
Total			100.00	100.00	

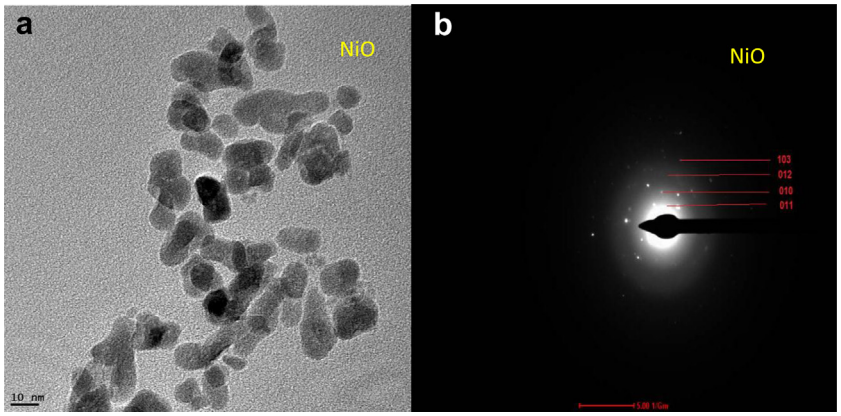

Fig. 2. (a) TEM, (b) SAED pattern analysis of NiO nanoparticles as prepared sample.

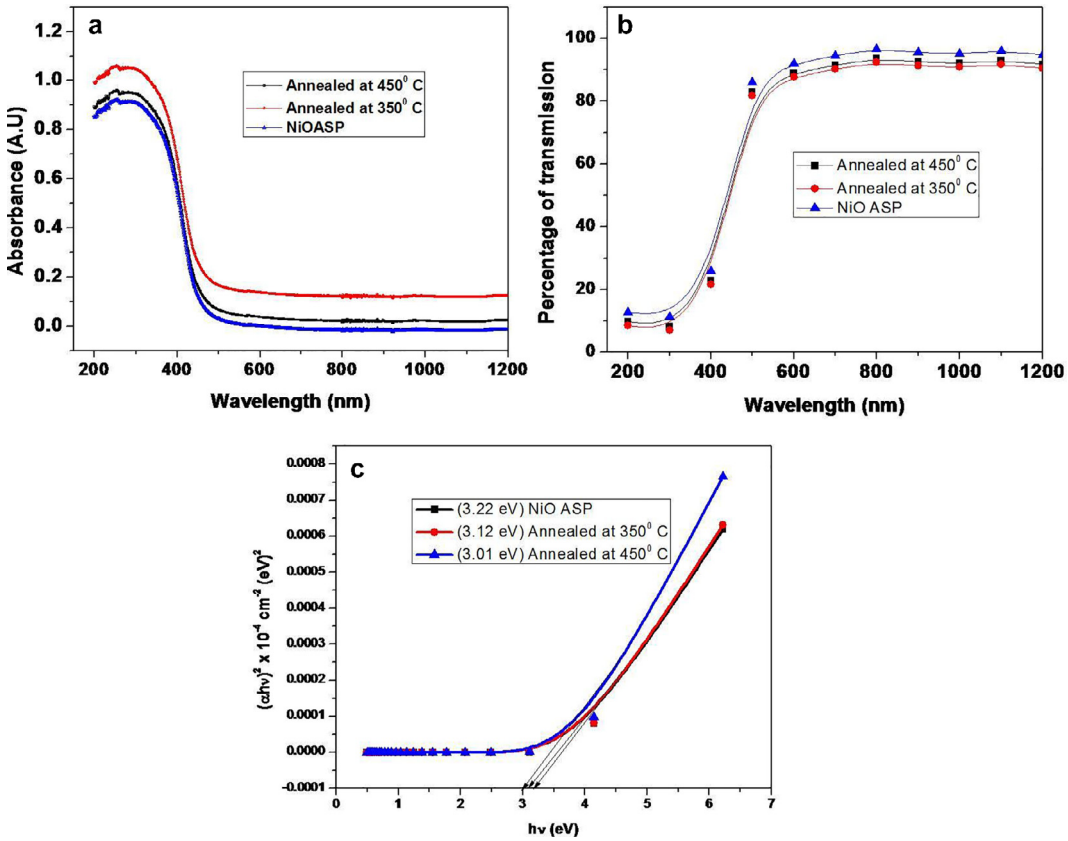

Fig. 3. Absorbance Curve (Band gap) of NiO (a) as prepared (b) 350 °C and (c) 450 °C samples.

$$a = \frac{\Delta d}{d_o} \tag{4}$$

d_{exp} and d_{hkl} represent the experimental and for standard values of inter planar distance respectively which are reported in (Table 1). Which is further noticed the value of increasing crystalline size in the range of 29.82, 32.14 and 33.24 nm, due to grain growth. According to formula (2), the smaller value of the crystallite size, the larger the value of the dislocation density (inversely proportional), which indicates a better crystalline quality. It can be seen that the dislocations density varies slightly with annealing temperature; it reduces about 30% when temperature increases up to 450 °C. In addition, when annealing temperature increases, the strain value increases, which is may be associated with the formation of oxygen vacancies [22]. Due to increase in annealing temperature, the oxygen ions are desorbed from the surface of the nanoparticles (low surface energy) and hence the concentration of oxygen vacancies increases, as evidenced from the EDAX analysis (Table 2).

$$\text{Hexagonal}\,\frac{1}{d^2} = \frac{4}{3}\left[\frac{h^2 + hk + k^2}{a^2}\right] + \frac{l^2}{c^2} \tag{5}$$

$$\text{Volume V} = \left(\frac{\sqrt{3a^2C}}{2}\right) \tag{6}$$

$$\text{Strain} = \beta\cos\theta/4 \tag{7}$$

The structure was said to be hexagonal in shape and the unit cell contains nearly 60 atoms and the lattice parameter was shown in (Table 1). This NiO structure resulted in series of oxygen network with various structural vacancies of oxygen. It means that the atom of oxygen present in structure should be recognised as interstrial atom molecule. Remaining unutilized oxygen were present in (0 1 1) unit cell directions. By comparing these diffractogram with the JCPDS data the phases present are the same for all the powdered particles.

Transmission Electron Microscope

The morphological studies of NiO were confirmed using microscopical technique From the Transmission Electron Microscope it was found that the average particle size to be 10 ± 2 nm (Fig. 2a, b). SAED pattern confirmed the crystalline diffraction planes and further it was well matched with XRD of NiO NPs diffraction patterns.

Band gap

The transmittance were found to be higher than 80% in the visible region, which slightly increases with further annealing, which is may be due to the better crystalline quality and larger grain size as evidenced for the XRD analysis and SEM observations. The optical band gap (E_g) of the NPs is estimated using by plot derived by Tauc's which were illustrated in (Fig. 3a, b), using the following relation:

$$(\alpha h\nu) = A(h\nu - Eg)^{n/2} \quad (8)$$

whereas α is denoted to be A coefficient of absorption which is said to be constant. The estimated (E_g) band gap optical is identified between 3.21 and 3.01 eV (Table 1). The band gap of optical property increases as the annealing temperature increases, which may be associated with desorption of oxygen from the surface of the powder as the concentration of carrier increases. The obtained band gap values are in agreement and within the range of the values reported in the literature [23].

The sample possesses an absorption edge around (370–390) nm. The absorption spectrum of NiO at 380 nm is due to charge-transfer from band of conduction to band of valance cations. Anatase shift in the absorption band toward shorter wavelength indicates decrease in particle size. At a primary step in the formation of the Oxide material is suggested to make a bond with the functional groups to induce metal nucleation. In this study oxide possesses a direct band gap system and the band gap energies of the oxide material were derived by Tauc's plot $E_g = (\alpha h\gamma)^2/(h\gamma)$ method which is depicted in Fig. 3c.

EDAX

Concentration of elements Ni and O varies periodically along the atoms size being accompanied with maxima of Ni along 51% and O along 49% of distributions (Table 2), there is no evidence of impurity in the composition. Fine particles tend to form agglomerates and fine spherical shape of powdered particles are frequently seen on the surface of coarser powders. From the SEM analysis the surface concentration of oxygen looks like coarse islands the height is also to be considered. The Ni atoms in the oxidized state are concentrated in the oxide form in the metallic state shown in (Fig. 4a,b) [24,25].

FT-IR analysis

The characteristic absorption peaks of oxide groups belong to 1116 cm $^{-1}$, 1388 cm^{-1} and 1454 cm^{-1} respecteveley. 2388 cm^{-1} indicates the presence of OH group. H_2O mode of bending at 1625 cm^{-1}, in the range of 3000–3700 cm^{-1} stretching mode is present one among another by O—H vibration mode of NiO at 2358 cm^{-1}. Strong absorption band at 1116 cm^{-1}, 3686 cm^{-1} and

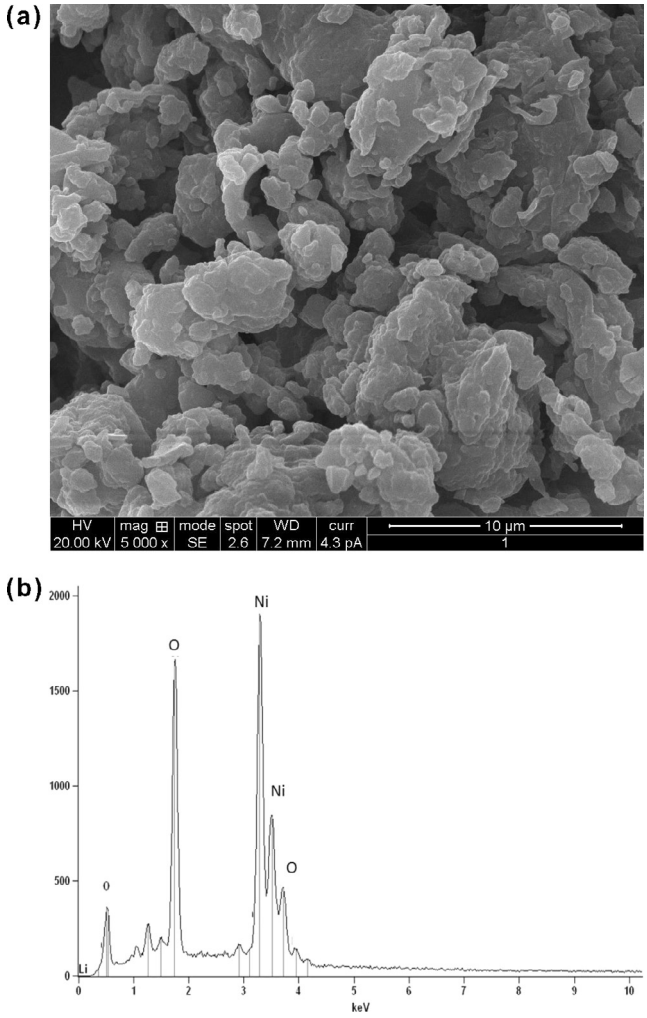

Fig. 4. (a) SEM analysis NiO NPs, (b) EDAX analysis NiO NPs.

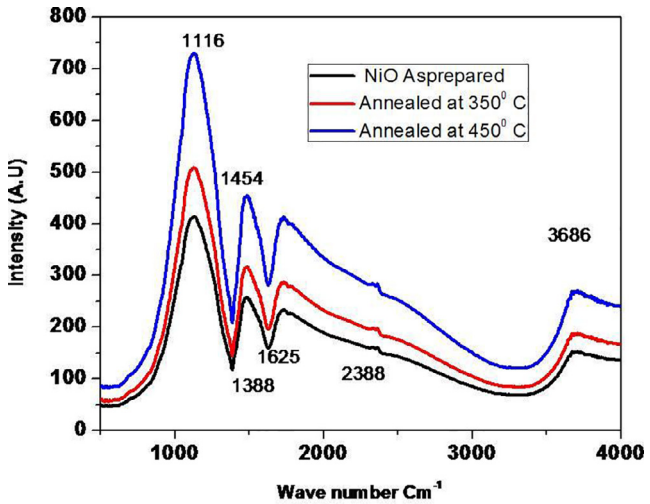

Fig. 5. FTIR analysis of NiO (i) as-prepared (ii) 350 °C and (iii) 450 °C samples.

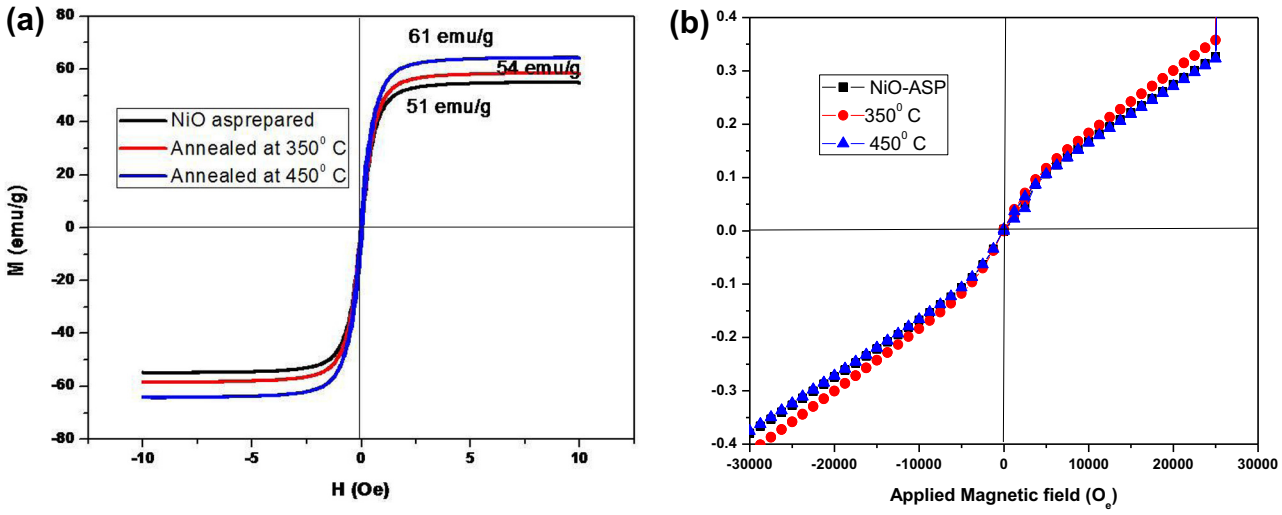

Fig. 6. Magnetization and coercivity values of (a) as prepared (b) 350 °C and 450 °C.

Table 3
Magnetic calculated parameters of NiO nanoparticles annealed at 350 °C and 450 °C.

	NiO	350 °C	450 °C
Coercivity (Hci) (G)	23.866	25.169	27.160
Magnetization (M) (emu/g)	52.505	54.826	61.369
Mass (mg)	1.0000	1.0000	1.0000
Retentivity (M_r) ($\times 10^{-3}$ emu/g)	46.173	47.236	48.325

2358 cm^{-1} belongs to (Ni—O) stretching frequencies respectively [26–28] (see Fig. 5).

Magnetic properties

The M-H curves of biosynthesized NiO NPs are well illustrated in (Fig. 6a, b). All the samples exhibit paramagnetic behaviour with some small ferromagnetic component. Slight hysteresis loop can be observed for all samples. The origin of room temperature ferromagnetism in metal oxides was associated to structural defects such as oxygen/metal vacancies as well as to the presence of secondary magnetic phases that can be formed during the synthesis. Latter can be ruled out because no secondary phase has been observed from XRD patterns. The weak ferromagnetism arises due to the exchange interaction between a pair of magnetic moment through oxygen vacancies which forms a bound magnetic polar [29,30]. The coercivity (G), magnetization (emu/g), Mass (mg) and retentively (emu/g) values of NiO as we prepared and annealed temperatures of 350 °C and 450 °C were tabulated in (Table 3).

Bacterial activities

The potential effects of the synthesized materials toward the suppression of the microbial pathogens such *Staphylococcus aureus*

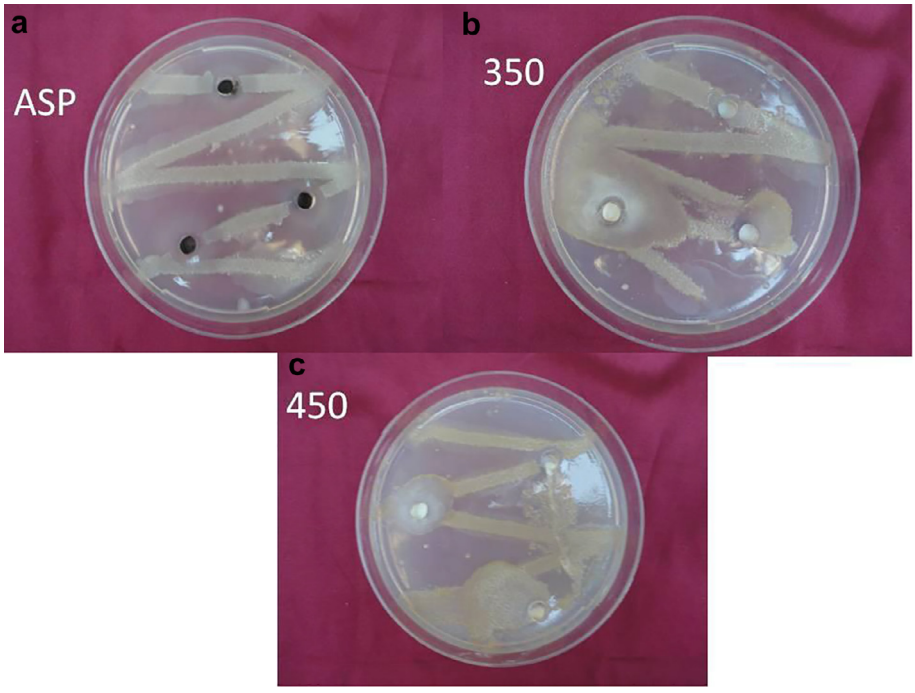

Fig. 7. Bacterial analysis of (a) ASP-NiO (b) 350 °C (c) 450 °C.

Table 4
Antibacterial activity analysis of NiO as-prepared and annealed samples.

Coating cycle	Zone of inhibition (3) in mm	
	E. coli MTCC6428 (+Ve)	*E. coli Bacillus* spp. *MTCC 739*
NiO	11	10
350 °C	13	11
450 °C	15	15
Coating cycle	Zone of inhibition (6) in mm	
	E. coli MTCC6428 (−Ve)	*E. coli Bacillus* spp. *MTCC 739*
NiO	11	10
350 °C	13	11
450 °C	15	15

and *Escherichia coli* was explored by well diffusion method. In details, the microbial strains were freshly cultivated in the nutrient broth and the mid log phase strains were spread on the nutrient agar plates and allowed for even distribution. Further the 10 mm well were made using sterile kork borer and the filtered compounds were transferred into the well for diffusion. Further, the sterile plates were incubated at 37 °C for 17 h. After incubation, the antimicrobial activity was measured with respect to the zone of inhibition. The experiment was repeated thrice for further confirmation of the antimicrobial activity by agar diffusion assay and Resazurin Microtitre Assay (REMA) (Sarker and Nahar 2007) [31–33]. Since *Staphylococcus aureus* and the *Escherichia coli* have been implies to be the important common pathogens in biomaterial-associated infections [34]. The antibacterial properties confirmed that the NiO NPs activities were resulted to be significantly better, whereas the activity said to be dependent of the concentration of the compounds (Fig. 7a–c) (Table 4). The antibacterial activity of NiO was comparable with *P. aeruginosa* and *E. coli* which evidenced that both strains were reported as the most pathogenic strains with high concentration of lipopolysaccharides [35–37]. The activity of NiO NPs and its annealing temperatures was moderate. Also, it is proved that NiO NPs might have penetrated the cell wall of the strains and altered the cellular membrane and inner cellular components which leads to the cell death. Similarly, few reports claimed that metal oxide completely inhibit the growth of the microbial pathogens.

Conclusion

In conclusion, NiO NPs was successfully synthesized via biosynthesis method using simple treatment of annealing temperatures. Further the analytical techniques like XRD, SEM and TEM confirms the biosynthesized NiO were in nano form with oblong shape of 12 nm in size. Further the applicational bacterial analysis of NiO confirms the synthesized nanoparticle consists of nanoholes with various pore size leads to heat treatment by precursor.

Conflicts of interest

All the authors states that there is no conflict of interest regarding this manuscript to publish in your reputed journal

Acknowledgements

The authors extend their sincere appreciation to the Deanship of Scientific Research at King Saud University for its funding this Prolific Research Group (PRG-1437-28).

References

[1] Elango G, Roopan SM, Irukatla K, Elumalai K, Al-Dhabi NA, Arasu MV. Spectroscopic investigation of biosynthesized nickel nanoparticles and its larvicidal, pesticidal activities. J Photochem Photobiol B. 2016;162:162–7.
[2] Hakim A, Hossain J, Khan KA. Temperature effect on the electrical properties of undoped NiO thin films. Renew Energy 2009;34:2625–9.
[3] Kumar R, Roopan SM, Prabhakarn A, Khanna VG, Chakroborty S. Agricultural waste *Annona squamosa* peel extract: biosynthesis of silver nanoparticles. Spectrochim Acta A 2012;90:173–6.
[4] Roopan SM, Bharathi A, Kumar R, Khanna VG, Prabhakarn A. Acaricidal, insecticidal, and larvicidal efficacy of aqueous extract of *Annona squamosa* L. peel as biomaterial for the reduction of palladium salts into nanoparticles. Colloid Surf B 2012;92:209–12.
[5] Madhumitha G, Rajakumar G, Roopan SM, Rahuman AA, Priya KM, Saral AM, et al. Acaricidal, insecticidal, and larvicidal efficacy of fruit peel aqueous extract of *Annona squamosa* and its compounds against blood-feeding parasites. Parasitol Res 2012;111:2189–99.
[6] Roopan SM, Kumar SHS, Madhumitha G, Suthindhiran K. Biogenic-production of SnO_2 nanoparticles and its cytotoxic effect against hepatocellular carcinoma cell line (HepG2). Appl Biochem Biotechnol 2014;175:1567–75.
[7] Kalaiselvi A, Roopan SM, Madhumitha G, Ramalingam C, Elango G. Synthesis and characterization of palladium nanoparticles using *Catharanthus roseus* leaf extract and its application in the photo-catalytic degradation. Spectrochim Acta A 2015;135:116–9.
[8] Elango G, Roopan SM. Green synthesis, spectroscopic investigation and photocatalytic activity of lead nanoparticles. Spectrochim Acta A 2015;139:367–73.
[9] Kumar DA, Palanichamy V, Roopan SM. One step production of AgCl nanoparticles and its antioxidant and photo catalytic activity. Mater Lett 2015;144:62–4.
[10] Haritha E, Roopan SM, Madhavi G, Elango G, Al-Dhabi NA, Arasu MV. Green chemical approach towards the synthesis of SnO_2 NPs in argument with photocatalytic degradation of diazo dye and its kinetic studies. J Photochem Photobiol B 2016;162:441–7.
[11] Roopan SM, Khan FRN. SnO_2 nanoparticles mediated non-traditional synthesis of biologically active 9-chloro-6,13-dihydro-7-phenyl-5H-indolo [3,2-c]-acridine derivatives. Med Chem Res 2011;20:732–7.
[12] Manivel P, Roopan SM, Kumar RS, Khan FN. Synthesis of 3 substituted isoquinolin-1-yl-2-(cycloalk-2-enylidene) hydrazines and their antimicrobial properties. J Chil Chem Soc 2009;54:183–5.
[13] Palaniraja J, Roopan SM. Iodine-mediated synthesis of indazolo-quinazolinones via a multi-component reaction. RSC Adv 2015;12:8640–6.
[14] Madhumitha G, Elango G, Roopan SM. Biotechnological aspects of ZnO nanoparticles: overview on synthesis and its applications. Appl Microbiol Biotechnol;2(100):571–81.
[15] Elango G, Roopan SM. Efficacy of SnO_2 nanoparticles toward photocatalytic degradation of methylene blue dye. J Photochem Photobiol B 2016;155:34–8.
[16] Zhi-Guo Y, Li-Ping Z, Yan-Min G, Zhi-Zhen Y, Bing-Hui Z. Preparation and band-gap modulation in MgxNi1-xO thin films as a function of Mg contents. Thin Solid Films 2011;519:5174–7.
[17] Hotovy I, Huran J, Spiess L, Hascik S. Preparation and characterization of NiO thin films for gas sensor applications. Vacuum 2007;58:300–7.
[18] Elp JV, Eskes H, Kuiperr P, Sawatzky GA. Electronic structure of Li-doped NiO. Phys Rev B 1992;45:1612–22.
[19] Kamal H, Elmaghraby EK, Ali SS, Abdel-Hady K. The electrochromic behavior of Nickel oxide films sprayed at different preparative conditions. Thin Solid Films 2005;483:330–9.
[20] Patil UM, Salunkhe RR, Gurav KV, Lokhande CD. Chemically deposited nanocrystalline NiO thin films for super capacitor application. Appl Surf Sci 2008;255:2603–7.
[21] Gokul B, Saravanan P, Vinod VTP, Cernik M, Sathyamoorthy R. Synthesis of Ni/NiO nanocomposites by hydrothermal-assisted polyol process and their magnetic properties as a function of annealing temperature. Powder Technol 2015;274:98–104.
[22] Ayeshamariam A, Kashif M, Arokiaraj S, Bououdina M, Sankaracharyulu MGV, Jayachandran M, et al. Bio-synthesis of NiO and Ni nanoparticles and their characterization. Dig J Nanomater Biostruct 2014;9(3):1007–19.
[23] Naz S, Qadir MI, Ali M, Janbaz KH. Nanotechnology for imaging and drug delivery in cancer. J Chem Soc Pak 2012;34:1.
[24] Baskoutas S, Terzis AF. Size dependent band gap of colloidal quantum dots, American Institute of Physics. J Appl Phys 2006;99:013708.
[25] Hill AW, Shears AL, Hibbitt KG. Increased antibacterial activity against *Escherichia coli* in Bovine serum after the induction of endotoxin tolerance. Am Soc Micro 1976;14:257–65.
[26] Nathanael AJ, Mangalaraj D, Chen PC, Ponpandian N. Mechanical and photocatalytic properties of hydroxyapatite/titania nanocomposites prepared by combined high gravity and hydrothermal process. Comp Sci Technol 2010;70:419–26.
[27] Soo-Hwan K, Lee HS, Ryu DS, Choi SJ, Lee DS. Antibacterial activity of silver-nanoparticles against *Staphylococcus aureus* and *Escherichia coli*, Korean. J Microbial Biotechnol 2011;39:77–85.
[28] Zhang HT, Ding J, Chow GM. Synthesis and characterizations of Ni–Fe@ spinel oxide core–shell nanoparticles. Mater Res Bull 2009;44:1195–9.

[29] Raposo M, Ferreira Q, Ribeiro PA, A guide for Atomic force microscopy analysis of soft condensed Matter, Modern research and educational topics in microscopy. In: Mendez-vilas A, Diaz J, editors. FORMATEX; 2007.
[30] Lee HU, Jeong YS, Park SY, Jeong SY, Kim HG, Cho CR. Surface properties and cell response of fluoridated hydroxyapatite/TiO_2 coated on Ti substrate. Curr Appl Phys 2009;9:528–33.
[31] Sarker SD, Nahar L, Kumarasamy Y. Microtitre plate based antibacterial assay incorporating resazurin as an indicator of cell growth, and its application in the in vitro antibacterial screening of phytochemicals. Methods 2007;42:321–4.
[32] Naz N, Iqbal MZ. Synthesis, spectroscopic and biological studies of transition metal complexes of novel Schiff bases derived from cephradine and sugars. Sci. Int. (Lahore) 2011;23:27–31.
[33] Nathanael J, Lee JH, Mangalaraj D, Hong SI, Rhee YH. Multifunctional properties of hydroxyapatite/titania bio-nano-composites: bioactivity and antimicrobial studies. Powder Technol 2012;228:410–5.
[34] Chen DP, Wang XL, Du Y, Ni S, Chen ZB, Liao X. Growth mechanism and magnetic properties of highly crystalline NiO nanocubes and nanorods fabricated by evaporation. Cryst Growth Des 2012;12:2842–9.
[35] Balaji A, Vellayappan MV, Jhon AA, Subramanian AP, Jaganathan SK, Selvakumar M, et al. Biomaterials based nano-applications of Aloe vera and its perspective, a review. RSC Adv 2015;105:86199–213.
[36] Arasu MV. In vitro antifungal, probiotic and antioxidant properties of novel *Lactobacillus plantarum* K46 isolated from fermented sesame leaf. Ann Microbiol 2014;64(3):1333–46.
[37] Ayeshamariam A, Sankaracharyulu GV, Kashif M, Hussain S, Bououdina M, Jayachandran M. Antibacterial activity studies of Ni and SnO_2 loaded chitosan beads. Mater Sci Forum 2015;832:110–22.